Thin Solid Films, *183* (1989) 33–48

ELECTRONIC STRUCTURE OF ULTRATHIN Si_nGe_n STRAINED SUPERLATTICES: THE POSSIBILITY OF DIRECT BAND GAPS

SVERRE FROYEN, D. M. WOOD AND ALEX ZUNGER
Solar Energy Research Institute, Golden, CO 80401 (U.S.A.)
(Received May 30, 1989)

We examine theoretically the structural and electronic properties of thin Si_nGe_n superlattices for $n = 1, 2, 4$ and 6, grown on (001) and (110)-oriented substrates. The increased repeat distance along the growth direction leads to folding of conduction band states to the $\bar{\Gamma}$ point of the superlattice Brillouin zone, resulting in a significant reduction in the minimum direct band gap. Transitions to these folded-in states can have non-zero dipole matrix elements because of (i) atomic relaxation, leading to the accommodation of distinct Si–Si and Ge–Ge bond lengths and (ii) the superlattice ordering potential. Our calculations show that superlattices grown coherently on a (001)Si substrate remain indirect band gap materials, with a minimum gap from $\bar{\Gamma}$ to $\bar{\Delta}$ (near the X point) of the f.c.c. Brillouin zone. We find, however, that increasing the lattice parameter a_s of the substrate will further reduce the direct band gap. For $a_s \geqslant \bar{a}$, where $\bar{a}$ is the average of the lattice constants for silicon and germanium, we predict a nearly direct band gap: for Si_6Ge_6 the indirect band gap for $a_s = \bar{a}$ is only ≈ 0.01 eV smaller than the direct band gap. The lowest conduction band states in this case are localized on the silicon sublattice. For (110)-oriented substrates, a similar degree of directness in the band gap can be achieved even on silicon.

1. INTRODUCTION

The most widely used semiconductors are the indirect band gap materials silicon and germanium. Most applications in optoelectronics, however, require semiconducting materials with direct band gaps. If silicon or germanium could somehow be manufactured with direct band gaps of the appropriate magnitude, their already mature technology could be harnessed in integrated optics. One way to modify the electronic structure of a material is to impose additional structural order, *e.g.* by ordering the atoms of a disordered alloy into a superlattice. Such order will modify the Brillouin zone of the material and may cause the electron energy bands to fold, making previously indirect transitions direct. This possibility has spurred the current interest in short-period superlattices of silicon and germanium[1–13], in particular superlattices grown in the [001] direction. Here X and points along the Δ symmetry direction fold to the center, $\bar{\Gamma}$, of the superlattice Brillouin zone, raising

0040-6090/89/$3.50

the possibility of a direct band gap material. Short periods are necessary to obtain significant oscillator strength for such folded, pseudodirect transitions; as the thickness increases, the transition matrix elements quickly approach their vanishing bulk values. Growth of such materials has recently become possible through molecular beam epitaxy. Pearsall *et al.*[1,8,11] studied electroreflectance of Si_nGe_n superlattices on (001)Si for $n = 1, 2, 4$ and 6 and observed new optical transitions at 0.76, 1.25, 1.70 and 2.31 eV for $n = 4$.

Motivated by these results, in 1986 we began studies of the electronic structure for such superlattices. In this paper we review earlier results, present results from pseudopotential calculations on actual superlattices, and discuss the physics necessary to understand the design criteria for a direct gap superlattice. The paper is organized as follows: Section 2 describes the first principles pseudopotential method, Section 3 gives results for structural properties and total energies, in Section 4 we describe the electronic structure of the superlattices emphasizing the underlying physics, and finally Section 5 contains a short summary and conclusions.

2. METHOD

We have used the first principles pseudopotential method[14,15] to calculate both total structural energies and electronic energy levels for the following Si_nGe_n superlattices: $n = 2$, 4 and 6 on (001)Si, $n = 4$ on germanium and lattice-matched (001) alloy substrates, and $n = 4$, 6 and 8 on (110)Si. In the [001]-oriented superlattices, n is equal to the number of monolayers in each sublayer. In the [110] superlattices, each monolayer contributes two atoms to the unit cell, hence the number of monolayers is $n/2$. Semirelativistic pseudopotentials are generated using Kerker's method[16], and the wave functions are expanded in plane waves with kinetic energies up to 12 rydbergs for total energies and 15 rydbergs for the electronic energy levels. The calculation is done self-consistently and the charge density is evaluated at the equivalent of six special k-points[17,18] (10 for the $n = 4$ [001] and $n = 4$ and $n = 8$ [110] superlattices) in the irreducible part of the f.c.c. Brillouin zone. Exchange and correlation are treated within the local density approximation[19,20] (LDA) using the electron gas data of Ceperley and Alder as parameterized by Perdew and Zunger[21]. Atomic positions are determined by total energy minimization[14,15]. The electronic structure is then computed for the equilibrium, minimum energy configuration. The LDA, with its well-known band gap problem[21], underestimates the conduction band energies. Fortunately, the lowest superlattice conduction bands derive only from silicon and germanium X states. We can therefore approximately correct for the LDA error, at least for these X-derived states, by shifting our calculated conduction band states upwards by 0.64 eV, as discussed in ref. 6.

3. STRUCTURAL PROPERTIES

We calculate equilibrium lattice constants of 5.41 and 5.61 Å for pure silicon and germanium respectively. The experimental values[22] are 5.430 and 5.657 Å.

Assuming that strain induced by the mismatch between silicon and germanium lattice constants is accommodated elastically, the Si_nGe_n superlattices will grow

coherently without misfit dislocations on a substrate. The lattice constants parallel to the substrate, $a_{\parallel}$, are therefore fixed by the substrate and, except for the lattice-matched systems, the superlattices deform in the perpendicular direction to relieve part of the strain. We find that all superlattices grown on silicon or germanium substrates deform by 3%, *i.e.* $c/a_{\parallel} = 1.03 \pm 0.01$ for silicon and $c/a_{\parallel} = 0.97 \pm 0.01$ for germanium substrates. The uncertainty is caused partly by numerical uncertainty in locating a shallow minimum in the total energy *vs.* $c/a_{\parallel}$, and partly by our underestimation of the lattice mismatch between bulk silicon and germanium. Interplanar relaxations restore the spacings in the silicon and germanium layers to very close to those for the pure constituents. For a Si(Ge) substrate virtually all the strain is taken up by the Ge(Si) layers. The Si–Ge interlayer distance is close to the average of the Si–Si and Ge–Ge interlayer spacings.

Our total energy calculations permit assessing superlattice stability. To within 3 meV all superlattices ([001] and [110]) grown on silicon substrates have the same energy per atom. The epitaxial formation energy δH, *i.e.* the total energy of the relaxed superlattice relative to equivalent amounts of silicon and germanium grown coherently on silicon, is likewise

$$\delta H^{(n)} = \frac{0 \pm 30\,\text{meV}}{\text{(Si–Ge) pair}}$$

The formation enthalpy relative to equivalent amounts of *bulk* silicon and germanium is

$$\Delta H^{(n)} = \frac{34 \pm 30\,\text{meV}}{\text{(Si–Ge) pair}}$$

Thus as long as coherent growth is maintained, superlattices of any period n can be grown with the same ease.

4. ELECTRONIC PROPERTIES

4.1. Qualitative physics

The common approach to superlattice electronic structure is to start with the band structure of the constituents and then apply effective mass, particle-in-a-box type descriptions. Such models rest on the identification of states in terms of their localization on a sublattice (silicon and germanium). However, our results show that very few states in these superlattices show appreciable localization on any sublattice, a reflection of the very narrow width of the layers. While the results of our first principles numerical calculations are, of course, independent of such approximations, it is still advantageous to analyze them in terms of simple conceptual models, so that their physical content becomes clear. We propose the following sequence.

(1) Start from the calculated energy bands of a $Si_{0.5}Ge_{0.5}$ alloy on a lattice-matched substrate. Here the average strain is zero and there are no superlattice effects. Figure 1(c) shows the electronic energy levels of the alloy at selected symmetry points calculated using the virtual crystal approximation (VCA); corresponding results for the constituents, silicon and germanium, are shown in

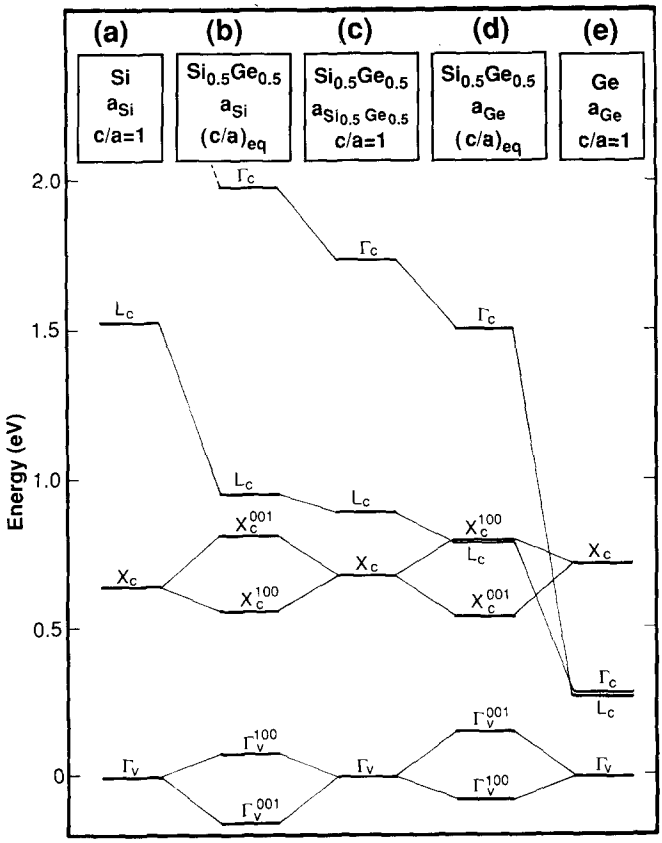

Fig. 1. Calculated LDA energy levels (in electronvolts) relative to the average of the strain split valence band maximum states at Γ, X and L of (a) bulk silicon (a_{Si} = 5.41 Å), (e) $Si_{0.5}Ge_{0.5}$ alloy (a_{SiGe} = 5.51 Å), and (e) germanium (a_{Ge} = 5.61 Å), as well as (b) and (d) [001] tetragonally distorted $Si_{0.5}Ge_{0.5}$ alloy. The calculated equilibrium lattice constants are used.

Figs. 1(a) and 1(e). The energy levels for the alloy occur at approximately the average of the corresponding levels for silicon and germanium. Since the L_c and Γ_c states of silicon are considerably above those of germanium, whereas the X_c states are low energy in both silicon and germanium, this averaging causes the alloy conduction bands at L and Γ to move upwards relative to the X states. The alloy becomes indirect from Γ to X and, as will be confirmed later, the states at L and Γ become irrelevant for the question of superlattice directness.

(2) Next we consider the effect of substrate-induced strain on the $Si_{0.5}Ge_{0.5}$ alloy. This is shown in Figs. 1(b) and 1(d), which show a VCA alloy grown on (001) silicon and germanium respectively. The alloy is now under compressive (Fig. 1(b)) or tensile (Fig. 1(d)) strain. We see that the tetragonal deformation associated with the substrate constraint removes the equivalence of the six X valleys. The two X valleys with their $\boldsymbol{k}$ vectors in the [001] directions (X_c^{001}), perpendicular to the substrate, shift up in energy with respect to the other four (X_c^{100}) for alloys on silicon

substrates and down for germanium substrates. Thus, in order to obtain a direct band gap when forming a superlattice, the superlattice-induced folding must be such that the lowest energy strain-split X band folds to $\bar{\Gamma}$.

The strain will also split the three-fold degeneracy (in the absence of spin-orbit splitting) of the valence band maximum into a doubly degenerate p^{100}, p^{010} pair and a single p^{001} state. Again the order of these states depends on the sign of the strain: for germanium substrates the singlet has the higher energy and forms the valence band maximum, and for silicon substrates the doublet is on top. The L states are not split by the strain.

(3) Now consider ordering of the $Si_{0.5}Ge_{0.5}$ alloy into a Si_nGe_n superlattice. The alloy states fold into the smaller superlattice Brillouin zone. For [001] superlattices, the [001]Δ line from Γ to X folds n times. Since the alloy X point is doubly degenerate, the superlattice can potentially have as many as $2n$ additional states at $\bar{\Gamma}$. To make the superlattice as nearly direct as possible, the substrate lattice constant should be chosen on the germanium side in order that the folding X_c^{001} state have lower energy than the non-folding X_c^{100} state (see Fig. 1(d)).

For superlattices grown in the [110] direction the [110] Σ line folds. The bands along this symmetry line in the first Brillouin zone are all higher energy states. However, [110] superlattices also have an increased repeat period (with respect to f.c.c.) along the [001] direction, causing the [001] X point to fold to $\bar{\Gamma}$. This raises the possibility[12] of a direct-gap [110] superlattice. Since the folding X point now has its $\boldsymbol{k}$ vector in the plane of the substrate, the effect of strain is reversed compared with the [001] superlattices, and [110] superlattices should be grown on silicon substrates to encourage directness. We verify this below.

The L states were not split by the strain, but the orthorhombic unit cell of the even-n superlattices (space group Pmma) causes the [111] and [$\bar{1}$11] L points to become inequivalent. For odd-n superlattices (space group I$\bar{4}$m2) they remain equivalent.

States which after folding have equal symmetry will repel one another. This effect is small for [001] but noticeable for [110] superlattices. Interestingly, it causes [111]-oriented $(AlAs)_n(GaAs)_n$ superlattices to be direct[23].

(4) Next, we must take into account the fact that the alloy conduction band minimum occurs not at X but along Δ at $k_{min} = 0.83k_X$, 0.19 eV below X_c. For the superlattices studied here, this minimum remains unfolded, possibly leading to a residual downward dispersion away from the folded-in Γ minimum. The dispersion will be modified by Brillouin zone edge effects and by the smaller size of the superlattice zone, and its magnitude will normally be much smaller than in the alloy. For [001] even-n Si_nGe_n superlattices, k_{min} folds provided $k_{min} = (n-2)/n \times k_X$. Choosing $n = 12$ will fold the alloy minimum to $\bar{\Gamma}$. A better choice might be to use odd-n superlattices. Here the X point does not fold and the condition above becomes $k_{min} = (n-1)/n \times k_X$, making $n = 5$ or seven good candidates for a true direct band gap material.

(5) Our superlattice calculations also predict band offsets for the Si/Ge interface. All our interfaces have the same strain-averaged valence band offset, 0.5 eV, with germanium higher in energy. This is in good agreement with the [001] offsets, 0.51–0.54 eV, calculated by Van de Walle and Martin[24] for various substrate

lattice constants. The conduction band offsets place the X^{001} conduction-band minimum on the silicon sublattice. For [001]-oriented superlattices, a large offset for the X_c^{001} states causes the lowest superlattice states at $\bar{\Gamma}$ to localized in the silicon region. For [110] superlattices, the offset is much smaller and the lowest $\bar{\Gamma}$ folding state is delocalized.

In the following we will label superlattice states with f.c.c. symmetry labels indicating the alloy origin of each state and adding an overbar to indicate that it is a superlattice state.

4.2. *[001]Si_nGe_n superlattices on silicon substrates*

We now turn to our calculated results for actual superlattices. We start with [001]Si_nGe_n superlattices grown on silicon substrates since these were the first to be studied experimentally[1]. In the random alloy, the relative position of the folding *vs.* the non-folding X states is completely determined by the tetragonal strain. In the superlattice, quantum confinement effects (*i.e.* the ability of the superlattice states to localize in the silicon or germanium regions of the system) will modify the simple

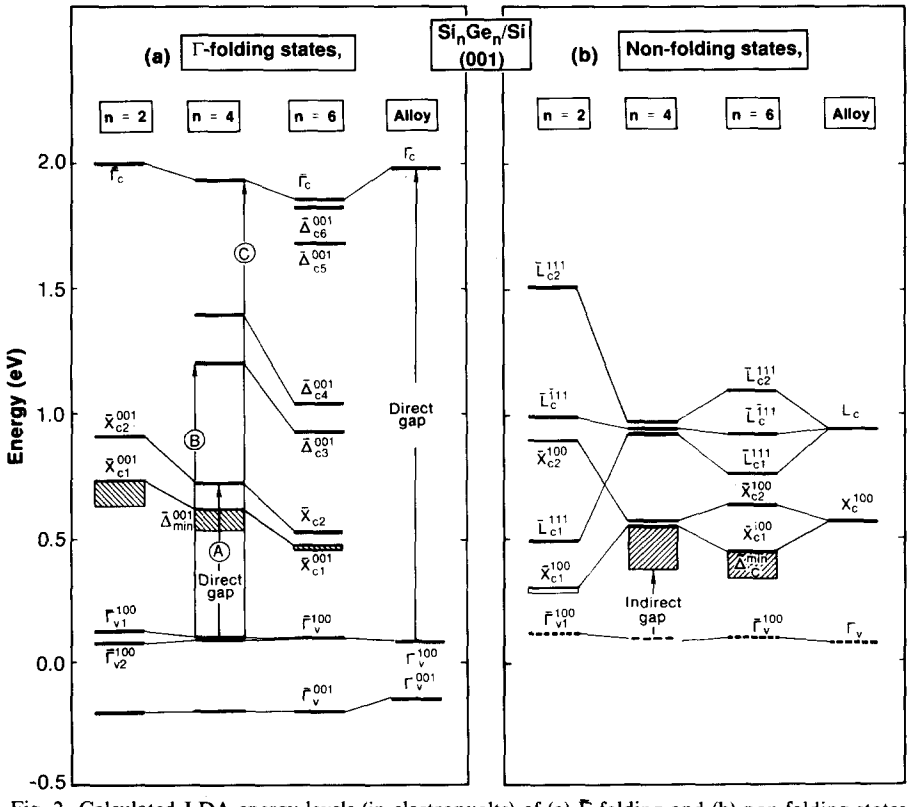

Fig. 2. Calculated LDA energy levels (in electronvolts) of (a) $\bar{\Gamma}$ folding and (b) non-folding states of strained [001] Si_nGe_n superlattices grown on silicon for $n = 2, 4$ and 6 and for the random $Si_{0.5}Ge_{0.5}$ alloy on silicon. Cross-hatched regions indicate the extent of downward dispersion of a band away from the symmetry point. The zero of energy is taken as the average of the top three valence states at Γ.

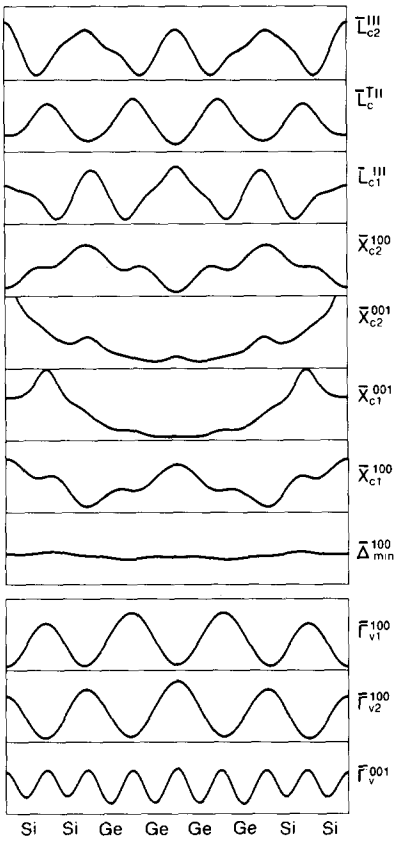

Fig. 3. (001) planar-averaged wave functions for selected states in the [001] Si_4Ge_4 superlattice on a silicon substrate.

arguments given in the previous section. Detailed calculations are therefore needed to predict the nature of the band gap confidently. Such results are shown in Figs. 2 and 3. We find that the superlattice conduction band states (Fig. 2) naturally divide into two categories: the $\bar{\Gamma}$ folding states (Fig. 2(a)), which behave as conventional quantum-confined states, and the non-folding states at $\bar{X}^{100}$ and $\bar{L}$ (Fig. 2(b)) which are delocalized in nature (see Fig. 3).

4.2.1. $\bar{\Gamma}$ folding states for [001]Si_nGe_n on silicon

Figure 2(a) shows the energies of states that fold to the center of the superlattice zone, $\bar{\Gamma}$. The valance band maximum is located here and is formed from the alloy Γ'_{25v} p states. They are split into a pair $\bar{\Gamma}^{100}_{v1}$, $\bar{\Gamma}^{100}_{v2}$ and singlet $\bar{\Gamma}^{001}_{v3}$ by substrate-induced strain. The pair is then slightly split because of the orthorhombic symmetry of the superlattice. These states are delocalized on both sublattices, but with a slight emphasis on the germanium sublattice (see Fig. 3) reflecting the fact that the valence band offset places the germanium valence band maximum above silicon[6].

The $\bar{\Gamma}$ folding conduction band states behave as conventional quantum-confined states in two respects. First, except for the $n = 2$ superlattice, they are

confined to the silicon sublattice, as can be seen by inspecting the $\bar{X}_{c1}^{100}$ and $\bar{X}_{c2}^{001}$ wave function amplitudes in Fig. 3. Secondly, the energy of the $\bar{\Gamma}$ folding states drops as the silicon sublayer thickness n increases. The localization on a single sublattice of these states (reflecting the heavy longitudinal electron mass at X) emphasizes the possibility of quantum confinement even in atomically thin superlattices. These $\bar{\Gamma}$ folding states are seen to occur in pairs, mirroring the original degeneracy at X.

For $n = 4$ and 6 the additional states along Δ which fold to $\bar{\Gamma}$ still leave the conduction band minimum along Δ unfolded. As discussed above, this leads to a downward dispersion of the lowest conduction band state away from $\bar{\Gamma}$ in the [001] direction. The magnitude of this dispersion is indicated in Fig. 2(a) by the boxed region.

Comparison of the direct transitions in the strained $Si_{0.5}Ge_{0.5}$ on silicon alloy with those of the strained superlattice reveals a dramatic change: whereas the lowest direct ($\Gamma_v \rightarrow \Gamma_c$) transitions in the strained alloy appear above 1.9 eV, four new direct transitions appear in the Si_4Ge_4 superlattice below this energy.

Since the new low energy conduction band states are folded-in states, they would normally be expected to have small transition matrix elements with the upper valence band states. (In the absence of superlattice ordering and atomic relaxations, such pseudodirect transitions carry no oscillator strength.) The transition matrix elements are, however, enhanced by the Si–Ge potential difference and by the different interplanar distances in the two sublayers. As the layers become thicker the matrix elements must decrease and approach their vanishing bulk values. This is clearly seen in Table I, where the squares on the matrix elements are tabulated. Notice that in the $n = 4$ superlattice the symmetry of the lower conduction band is opposite that of the $n = 2$ and 6 superlattices and all transitions to the lowest conduction band state are dipole forbidden.

We see that for parallel polarization, corresponding to the experimental situation in ref. 1, we expect three groups of transitions for $n = 4$, denoted A, B and C in Fig. 2(a). Their LDA energies (Table I) are 0.63, 1.11 and 1.84, respectively. Correcting approximately for the LDA error (see Section 2), this gives,

$$\bar{\Gamma}_{v1,2}^{100} \rightarrow \bar{X}_{c2}^{001} = 1.27 \pm 0.04\,\text{eV} \quad \text{(A)}$$

$$\bar{\Gamma}_{v1,2}^{100} \rightarrow \bar{\Delta}_{c3}^{001} = 1.75 \pm 0.04\,\text{eV} \quad \text{(B)}$$

$$\bar{\Gamma}_{v1,2}^{100} \rightarrow \bar{\Gamma}_{c}^{001} = 2.6 \pm 0.3\,\text{eV} \quad \text{(C)}$$

We assign transition A to that observed[1] at 1.25 eV (with a line width of 0.24 eV). Transition B, not seen in the original experiment, was later observed[8,11] at 1.70 eV. We assign the alloy-derived transition C to the one observed[1] at 2.31 eV (line width of 0.24 eV). The transition observed[1] at 0.76 eV is not a direct transition according to our calculation. It could correspond to the indirect $\bar{\Gamma}_v^{100} \rightarrow \bar{\Delta}_{min}^{001}$ transition we calculate at 0.92 ± 0.04 eV after correcting for the LDA error. It is also possible, given the small thickness of the overall superlattice, that the observed transition is from the superlattice $\bar{\Gamma}_v$ state to the conduction band minimum of the silicon substrate. Such a transition would be 0.19 eV lower in energy than the $\bar{\Gamma}_v^{100} \rightarrow \bar{\Delta}_{min}^{001}$ transition and therefore closer to the observed value (see Fig. 11 and Section VI in ref. 6.)

TABLE I

CALCULATED TRANSITION ENERGIES ΔE AND DIPOLE MATRIX ELEMENTS, $|\langle i|\hat{e}\cdot\vec{r}|f\rangle|^2$ FOR [001] Si_nGe_n SUPERLATTICES WITH $n = 2, 4$ AND 6 ON A SILICON SUBSTRATE. (THE VALUES FOR A GERMANIUM SUBSTRATE ARE GIVEN IN PARENTHESES FOR $n = 4$.) $\langle i|$ IS A VALENCE STATE AND $|f\rangle$ A CONDUCTION BAND STATE AS INDICATED; α IS THE DIRECTION OF POLARIZATION. THE NOTATION FOR THE STATES REFER TO FIG. 2. EACH TRANSITION HAS A NON-ZERO MATRIX ELEMENT FOR A GIVEN POLARIZATION, $\hat{e}$, ONLY. THE MATRIX ELEMENTS HAVE BEEN NORMALIZED SO THAT THE STRONG, $\Gamma'_{25v} \rightarrow \Gamma'_{2c}$ DERIVED TRANSITION IS UNITY. ENERGY DIFFERENCES ARE IN ELECTRONVOLTS

$\langle i\|$	$\|f\rangle$	$\bar{\Gamma}_v^{001}$ ($\hat{e} = 001$)		$\bar{\Gamma}_{2v}^{100}$ ($\hat{e} = 100/010$)		$\bar{\Gamma}_{1v}^{100}$ ($\hat{e} = 100/010$)	
n		$\|\langle\hat{e}\cdot\vec{r}\rangle\|^2$	ΔE	$\|\langle\hat{e}\cdot\vec{r}\rangle\|^2$	ΔE	$\|\langle\hat{e}\cdot\vec{r}\rangle\|^2$	ΔE
2	$\bar{X}_{1c}^{001}$	0.21	0.93	1.28	0.65	0.07	0.61
	$\bar{X}_{2c}^{001}$	0	1.11	0	0.83	0	0.79
	$\bar{\Gamma}_c$	1	2.30	1	2.02	1	1.98
4	$\bar{X}_{1c}^{001}$	0	0.80 (0.24)	0	0.53 (0.43)	0	0.52 (0.41)
	$\bar{X}_{2c}^{001}$	0.02 (0.08)	0.91 (0.34)	0.04 (0.05)	0.63 (0.53)	≈ 0 (0.02)	0.63 (0.52)
	$\bar{\Delta}_{3c}^{001}$	0.04 (0.06)	1.39 (0.79)	0.12 (0.08)	1.11 (0.97)	≈ 0 (≈ 0)	1.11 (0.96)
	$\bar{\Delta}_{4c}^{001}$	0	1.58 (0.95)	0	1.30 (1.13)	0	1.30 (1.12)
	$\bar{\Gamma}_c$	1	2.12 (1.39)	1	1.84 (1.57)	1	1.84 (1.56)
6	$\bar{X}_{1c}^{001}$	0.01	0.67	0.11	0.37	≈ 0	0.37
	$\bar{X}_{2c}^{001}$	0	0.73	0	0.43	0	0.43
	$\bar{\Delta}_{3c}^{001}$	0	1.13	0	0.83	0	0.83
	$\bar{\Delta}_{4c}^{001}$	0.03	1.24	0.10	0.94	0.01	0.94
	$\bar{\Delta}_{5c}^{001}$	0.04	1.88	0.11	1.59	≈ 0	1.59
	$\bar{\Delta}_{6c}^{001}$	0	2.02	0	1.72	0	1.72
	$\bar{\Gamma}_c$	1	2.05	1	1.75	1	1.75

4.2.2. Non-folding states for [001] Si_nGe_n on silicon

Figure 2(b) shows, for a silicon substrate, the variation in the indirect band gap states with the superlattice period n. The non-folding $\bar{X}^{100}$, $\bar{L}^{111}$ and $\bar{L}^{\bar{1}11}$ states are extended on both silicon and germanium sublayers (see Fig. 3). The fourfold degeneracy of the alloy X_c^{100} state (twice the f.c.c. value because of zone folding) is split by the superlattice potential into upper and lower pairs.

The doubly degenerate L point is split at $\bar{L}^{111}$ into $\bar{L}_{c1}^{111}$ and $\bar{L}_{c2}^{111}$ but remains degenerate at $\bar{L}^{\bar{1}11}$. Figure 2(b) shows that the splitting of the $\bar{L}_{c1}^{111}$ and $\bar{L}_{c2}^{111}$ states oscillates with n, exhibiting a large energy difference for $n = 2$ and 6 and near degeneracy for $n = 4$. This variation with n has been shown[6] to be a measure of the commensurability of the superlattice period with the period of the wavefunctions. The underlying period of the wavefunctions is four monolayers. Thus the lattice is in perfect registry with the wavefunction in the $n = 2$ superlattice and the states are able to sample fully the difference between the silicon and germanium potentials. For $n = 4$ the states are forced to sample both sublattices equally and the splitting is close to zero. For $n = 6$ each wavefunction can place two-thirds of its weight on one

sublattice and one-third on the other, giving one-third of the splitting of the $n = 2$ superlattice. In general the splitting is zero for n a multiple of four. For other n the wavefunction has relative amplitude of $2/n$ and $(n-2)/n$ on the two sublattices, leading to a splitting $2/n$ times that for $n = 2$. Because of their delocalized nature, the average of the states changes only slightly with n, although for sufficiently thick layers the states will localize and their energy will drop. This non-monotonic behavior of the superlattice $\bar{L}^{111}$ and $\bar{X}^{100}$ conduction band energies, coupled with the small variations with n we find for the corresponding valence band energies, suggests that the energy of direct $\bar{X}_v \rightarrow \bar{X}_c$ and $\bar{L}_v \rightarrow \bar{L}_c$ transitions should be non-monotonic as a function of n. Our calculations (corrected for LDA errors) predict $\bar{X}_c - \bar{X}_v$ splitting of 4.07, 4.37 and 4.28 (± 0.04) eV, and $\bar{L}_c - \bar{L}_v$ splitting of 1.95, 2.45 and 2.30 (± 0.12) eV for $n = 2$, 4 and 6 respectively. Experimental testing of this prediction is lacking.

4.3. [001] Si_4Ge_4 superlattices on other substrates

In all the superlattices described so far, the indirect states at $\bar{X}_{c1}^{100}$ are well below the Γ folding $\bar{X}_{c1}^{001}$ states. This makes all of these superlattices indirect band gap systems. The origin of this (the tetragonal deformation imposed by the substrate) was discussed in Section 4.1. If the substrate lattice constant is increased, the tetragonal strain changes sign, and the order of $\bar{X}_{c1}^{001}$ and $\bar{X}_{c1}^{100}$ in Fig. 2 should be reversed (compare with Figs. 1(b) and 1(d)). To test this hypothesis, we performed two calculations: one for an $n = 4$ superlattice with a substrate lattice constant equal to the average of silicon and germanium (appropriate for a superlattice grown on a $Si_{0.5}Ge_{0.5}$ alloy substrate or for a free-standing superlattice), and the other for an $n = 4$ superlattice on germanium. Results for these calculations are shown in Fig. 4.

We observe that as the substrate lattice constant increases, the $\bar{X}_{c1}^{100}$ and $\bar{\Delta}_{min}^{100}$ states shift up in energy with respect to the $\bar{\Gamma}$ folding states at $\bar{X}_c^{001}$. For an alloy substrate this shift is already sufficient to place the previous minimum at $\bar{\Delta}_{min}^{100}$ above the lowest direct conduction band at $\bar{X}_{c1}^{001}$. The $n = 4$ superlattices remain indirect, however, because of the 0.1 eV downward dispersion away from $\bar{\Gamma}$ in the [001] direction. The magnitude of this dispersion can be reduced by increasing n. For $n = 6$ it is already only 0.01 eV (see Fig. 2(a)) and for even-n superlattices with $n = 10$ or 12 or odd-n superlattices with $n = 5$ or 7 it should vanish completely as the minimum of the alloy's first conduction band folds to $\bar{\Gamma}$ (see Section 4.1). Zachai *et al.*[13] have recently observed strong photoluminescence from a Si_6Ge_4[001] superlattice grown on a lattice-matched ("strain-symmetrized") substrate, suggesting that this is a direct band gap material in agreement with our prediction.

The growth of Si_nGe_n on a lattice-matched alloy substrate is facilitated by the smaller strain in the layers (2%) relative to the situation with a silicon or germanium substrate (4%). An added advantage is that since the superlattice on the average is lattice matched, there is no limit on the total thickness of the superlattice and the growth of optical thicknesses should be possible.

4.4. [110] Si_nGe_n superlattices on silicon substrates

As discussed in Section 4.1, for superlattices grown in the [110] direction the effect of strain on the $\bar{\Gamma}$ folding X^{001} states is reversed. To investigate this possibility

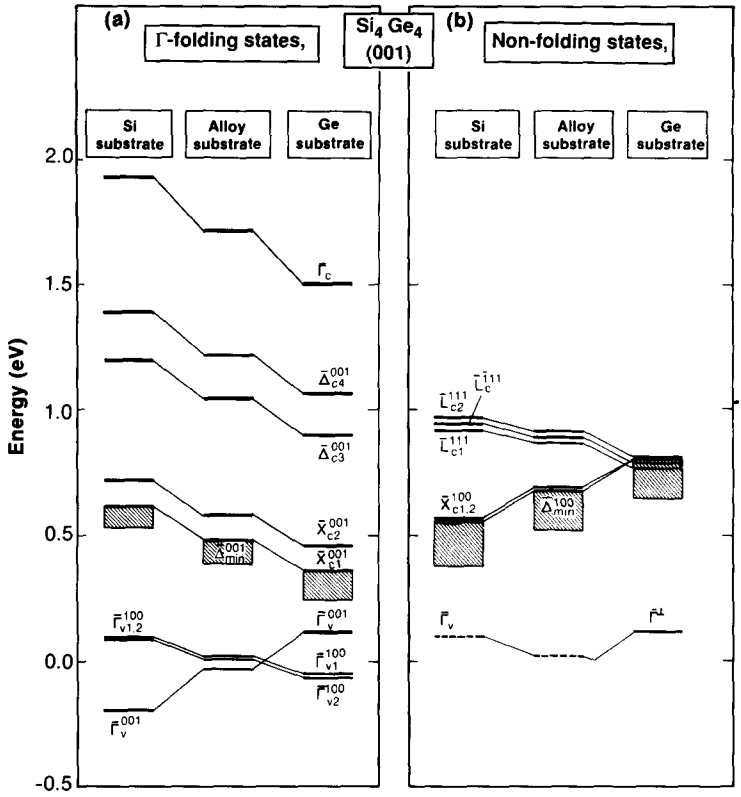

Fig. 4. Calculated LDA energy levels (in electronvolts) of (a) $\bar{\Gamma}$ folding and (b) non-folding states of [001] Si_4Ge_4 superlattices matched epitaxially to silicon, a $Si_{0.5}Ge_{0.5}$ alloy, and germanium substrates. Cross-hatched regions indicate the extent of downward dispersion of a band away from the symmetry point. The zero of energy is taken as the average of the top three valence states at $\bar{\Gamma}$.

for a direct band gap superlattice on a silicon substrate, we have performed calculations for Si_nGe_n[110] superlattices on silicon for $n = 4$, 6 and 8. The results are shown in Figs. 5 and 6. Figure 5 shows calculated band energies at symmetry points for the superlattices. We also show (as $n = \infty$) values appropriate for a Si/Ge interface, *i.e.* calculated band offsets. The band energies for each superlattice have been appropriately aligned so that any band offset can be read off the figure. Figure 6 shows planar-averaged wavefunctions $|\psi|^2$ for the $\bar{\Gamma}$ folding states in the $n = 6$ superlattice. We next discuss separately the $\bar{\Gamma}$ folding and the nonfolding states.

4.4.1. $\bar{\Gamma}$-folding states for [110] Si_nGe_n on silicon

Figure 5(a) shows the energies of states that fold to the center of the superlattice zone, $\bar{\Gamma}$. Again the valence band maximum is located here. The states are now completely split by the substrate-induced strain as well as by interaction between folded-in states of the same symmetry. The uppermost valence band state, $\bar{\Gamma}_{v1}$, is localized on the germanium sublattice (see Fig. 6(c)) and its energy approaches the germanium valence band edge as the superlattice thickness increases.

The lowest conduction band at $\bar{\Gamma}$, $\bar{X}_{c1}^{001}$, is formed by a folded-in [001] $\bar{X}$ state.

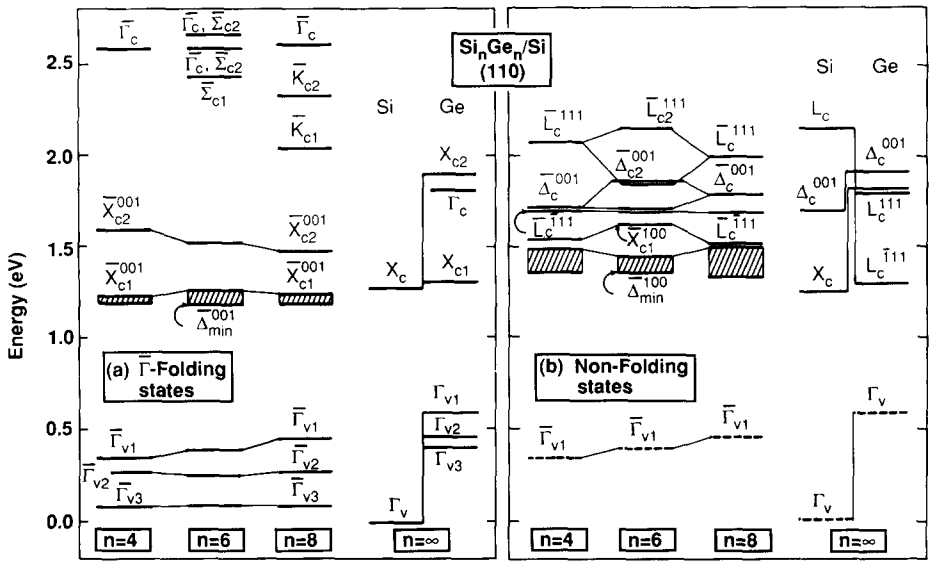

Fig. 5. Calculated energy levels (in electronvolts) of (a) $\bar{\Gamma}$ folding and (b) non-folding states for strained [110] Si_nGe_n superlattices grown on silicon for $n = 4$, 6 and 8 and for the superlattice constituents silicon and germanium. Cross-hatched regions indicate the extent of downward dispersion of a band away from the symmetry point. The energy levels for the different superlattices have been aligned using calculated band offsets and the conduction band energies have been shifted 0.64 eV upwards to approximately correct for LDA errors.

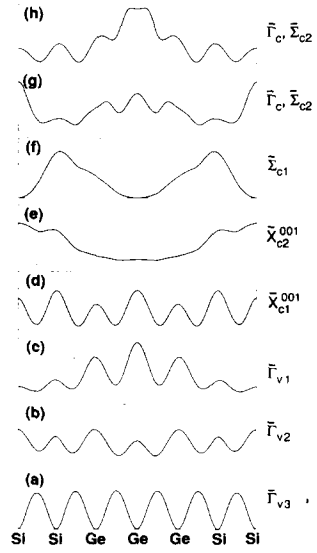

Fig. 6. (110) planar-averaged wave functions for $\bar{\Gamma}$ folding states in the [110] Si_6Ge_6 superlattice on a silicon substrate.

TABLE II

SYMMETRY LABELS FOR $\bar{\Gamma}$ FOLDING STATES IN [110] Si_nGe_n SUPERLATTICES, POINT GROUP SYMMETRY mmm. THE SYMMETRY NOTATION IS FROM TINKHAM[26]

State	*Symmetry*		
	$n = 4$	$n = 6$	$n = 8$
$\bar{\Gamma}_c$	B_{1u}	B_{1u}	B_{1u}
$\bar{\Sigma}_{c2}, \bar{K}_{c2}$		B_{1u}	B_{2g}
$\bar{\Sigma}_{c1}, \bar{K}_{c1}$		B_{2g}	B_{1u}
$\bar{X}^{001}_{c2}$	B_{2g}	B_{1u}	B_{2g}
$\bar{X}^{001}_{c1}$	B_{3u}	A_{1g}	B_{3u}
$\bar{\Gamma}_{v1}$	B_{3g}	B_{3g}	B_{3g}
$\bar{\Gamma}_{v2}$	A_{1g}	A_{1g}	A_{1g}
$\bar{\Gamma}_{v3}$	B_{2g}	B_{2g}	B_{2g}

The symmetry of this state (see Table II) changes with n, causing a small shift upwards for $n = 6$ as it interacts with the valence band state $\bar{\Gamma}_{v2}$. This is also seen in the complementary nature of the wavefunctions (see Figs. 6(b) and 6(d)). There is a small residual downward dispersion immediately away from $\bar{\Gamma}$, reflecting the downward dispersion from X to the conduction band minimum at Δ in the alloy. This dispersion is indicated by the shaded area in Fig. 5(a), and amounts to 35, 72 and 50 meV for $n = 4$, 6 and 8 respectively. For comparison, the dispersion of the folded-in [001] X states in [001]-oriented superlattices is 99, 85 and 12 meV for $n = 2$, 4 and 6 grown on silicon and 114 meV for the $n = 4$ superlattice grown on germanium. The folding of states along the superlattice direction Σ does not lead to low energy states until $n = 6$, when a point close to K folds, and $n = 8$, when the K point itself folds. For $n = 6$, the folding state labeled $\bar{\Sigma}_{c2}$ interacts strongly with the original alloy Γ'_{2c} state (both of B_{1u} symmetry), making identification of their origins in alloy states impossible. The $\bar{\Gamma}$ folding conduction band states are delocalized with the exception of the $\bar{X}^{001}_{c2}$ state, which is localized on the silicon sublattice, and the upper of the $\bar{\Gamma}_c$, $\bar{\Sigma}_{c2}$ pair, which is localized on the germanium sublattice (see Figs. 6(e) and 6(g)).

Table III shows calculated dipole matrix elements for the $\bar{\Gamma}$ folding states up to and including the alloy Γ state at about 2 eV. Matrix elements for transitions to states folded from the [001] X point are smaller than those folded from the Σ or K points and are much smaller for $n = 4$ and 8. This can be understood by considering the orientation dependence of the ordering potential: the difference between the potentials of the ordered superlattice and of the disordered alloy after planar averaging in a given direction. Assigning constant potentials V_{Si} to the silicon layers and V_{Ge} to the germanium layers, we can approximate the ordering potentials as follows. In the [110] direction the ordering potential is simply the difference $V_{Si} - V_{Ge}$, independent of the repeat period. In the [001] direction, responsible for the folding of the [001] X point, the ordering potential is $2(V_{Si} - V_{Ge})/n$ for $n = 2$, 6, 10, etc., and zero otherwise. This explains the extraordinary small matrix elements for n

TABLE III

CALCULATED TRANSITION ENERGIES ΔE AND DIPOLE MATRIX ELEMENTS $|\langle i|\hat{e}\cdot\vec{r}|f\rangle|^2$ IN [110] Si_nGe_n SUPERLATTICES FOR $n = 4$, 6 AND 8 ON A SILICON SUBSTRATE. EACH TRANSITION HAS A NON-ZERO DIPOLE MATRIX ELEMENT FOR THE GIVEN POLARIZATION, $\hat{e}$, ONLY. THE NOTATION FOR THE STATES REFER TO FIG. 5. THE TRANSITION ENERGIES ARE IN ELECTRONVOLTS AND CAN BE APPROXIMATELY CORRECTED FOR LDA ERRORS BY ADDING 0.64 eV

$\langle i\|$		Γ_{v1}			Γ_{v2}			Γ_{v3}		
n	$\|f\rangle$	ΔE	$\|\langle\hat{e}\cdot\vec{r}\rangle\|^2$	$\hat{e}$	ΔE	$\|\langle\hat{e}\cdot\vec{r}\rangle\|^2$	$\hat{e}$	ΔE	$\|\langle\hat{e}\cdot\vec{r}\rangle\|^2$	$\hat{e}$
4	$\bar{X}_{c1}^{001}$	0.24	0.0		0.32	7.2×10^{-5}	[110]	0.50	4.8×10^{-5}	[001]
	$\bar{X}_{c2}^{001}$	0.61	0.0		0.69	0.0		0.87	0.0	
	$\bar{\Gamma}_c$	1.60	3.0×10^{-2}	[110]	1.68	7.0×10^{-2}	[001]	1.86	0.12	[110]
6	$\bar{X}_{c1}^{001}$	0.22	0.0		0.37	0.0		0.53	0.0	
	$\bar{X}_{c2}^{001}$	0.48	1.5×10^{-3}	[$\bar{1}$10]	0.63	1.0×10^{-3}	[001]	0.79	8.5×10^{-3}	[110]
	$\bar{\Sigma}_{c1}$	1.39	0.0		1.54	0.0		1.70	0.0	
	$\bar{\Gamma}_c, \bar{\Sigma}_{c2}$	1.55	1.9×10^{-2}	[$\bar{1}$10]	1.70	2.9×10^{-2}	[001]	1.86	5.9×10^{-2}	[110]
	$\bar{\Gamma}_c, \bar{\Sigma}_{c2}$	1.63	2.8×10^{-2}	[$\bar{1}$10]	1.77	3.9×10^{-2}	[001]	1.94	7.0×10^{-2}	[110]
8	$\bar{X}_{c1}^{001}$	0.15	0.0		0.33	4.1×10^{-6}	[110]	0.51	1.1×10^{-5}	[001]
	$\bar{X}_{c2}^{001}$	0.38	0.0		0.56	0.0		0.74	0.0	
	$\bar{K}_{c1}$	0.94	4.3×10^{-3}	[$\bar{1}$10]	1.12	8.5×10^{-3}	[001]	1.31	1.5×10^{-2}	[110]
	$\bar{K}_{c2}$	1.23	0.0		1.41	0.0		1.60	0.0	
	$\bar{\Gamma}_c$	1.51	6.1×10^{-2}	[$\bar{1}$10]	1.69	7.0×10^{-2}	[001]	1.88	0.12	[110]

$= 4$ and 8, and why they are orders of magnitude larger for $n = 6$. Unfortunately, the lowest energy dipole transitions in the $n = 6$ superlattice are symmetry forbidden.

For the new optically allowed transitions the LDA corrected energies are 0.96 and 1.14 eV (for $n = 4$), 1.12, 1.27 and 1.43 eV (for $n = 6$), and 0.97 and 1.15 eV (for $n = 8$). The minimum indirect gaps (to $\bar{\Delta}_{min}^{001}$) are 0.74, 0.97 and 0.89 eV respectively.

4.4.2. Non-folding states for [110] Si_nGe_n on silicon

Low energy non-folding states are shown in Fig. 5(b). These are derived from the various alloy Δ, X and L points and are labeled accordingly. $\bar{\Delta}_{min}^{100}$ is the conduction band minimum along [100] and [010] directions and $\bar{\Delta}_{c1}^{001}$ and $\bar{\Delta}_{c2}^{001}$ are states folded from $[001]\pi/a$. Comparing Figs. 5(a) and 5(b) we see that the $\bar{\Gamma}$ folding [001] $\bar{X}_{c1}^{001}$ state is indeed below all non-folding $\bar{X}$, $\bar{\Delta}$ and $\bar{L}$ states. The downward dispersion immediately away from $\bar{\Gamma}$ still leaves the superlattice indirect, but its small magnitude (35 meV for $n = 4$) makes this superlattice quasi-direct at room temperature.

4.5. Spin–orbit coupling

Our calculation does not include spin–orbit coupling, although qualitative features can be estimated from perturbation theory.[25] Its main effect is to couple the top three states, $\bar{\Gamma}_{v1-3}$, at the valence band maximum. This can make dipole forbidden transitions weakly allowed, and can shift the top valence band state upwards by at most $\Delta_0/3$, where Δ_0 is the spin–orbit splitting at the valence band maximum for the unstrained solid: 0.04 eV for silicon, 0.30 eV for germanium, and about 0.17 eV for the superlattices (the average of the constituents). This shift

reduces the direct band gap and slightly modifies the valence band offsets. The effect of spin–orbit on the confinement of the superlattice states is thus expected to be small.

5. CONCLUSIONS

We have shown that short-period Si–Ge superlattices exhibit new low energy optical transitions and that they are excellent candidates for direct band gap materials. Superlattices oriented in the [001] direction show the highest promise to be direct. Because of the strain splitting of the X valleys, they should be grown on Si/Ge alloy (with more than 50% germanium) or germanium substrates. If a silicon substrate must be used, superlattices grown in the [110] direction exhibit quasi-direct band gaps, i.e. $\bar{\Gamma}$ is lower in energy than $\bar{X}$, but the superlattice is nevertheless indirect because of a small downward dispersion (of the order $k_B T$) of the lowest conduction band away from $\bar{\Gamma}$.

ACKNOWLEDGMENT

We acknowledge the support of Department of Energy, Office of Energy Research, Basic Energy Sciences computer time under grant number DE-AC02-77CH00178.

REFERENCES

1 T. P. Pearsall, J. Bevk, L. C. Feldman, A. Ourmazd, J. M. Bonar and J. P. Mannaerts, *Phys. Rev. Lett.*, *58* (1987) 729.
2 R. People and S. A. Jackson, *Phys. Rev. B*, *36* (1987) 1310.
3 S. Froyen, D. M. Wood and A. Zunger, *Phys. Rev. B*, *36* (1987) 4547.
4 L. Brey and C. Tejedor, *Phys. Rev. Lett.*, *59* (1987) 1022.
5 M. S. Hybertsen and M. Schluter, *Phys. Rev. B*, *36* (1987) 9683.
6 S. Froyen, D. M. Wood and A. Zunger, *Phys. Rev. B*, *37* (1988) 6893.
7 K. B. Wong, M. Jaros, I. Morrison and J. P. Hagon, *Phys. Rev. Lett.*, *60* (1988) 2221.
8 M. S. Hybertsen, M. Schluter, R. People, S. A. Jackson, D. V. Lang, T. P. Pearsall, J. C. Bean, J. M. Vandenberg and J. Bevk, *Phys. Rev. B*, *37* (1988) 10195.
9 S. Satpathy, R. M. Martin and C. G. Van de Walle, *Phys. Rev. B*, *38* (1988) 13237.
10 G. Abstreiter, K. Eberl, E. Friess, W. Wegscheider and R. Zachai, *J. Cryst. Growth*, *95* (1989) 431.
11 T. P. Pearsall, J. Bevk, J. C. Bean, J. Bonar, J. P. Mannaerts and A. Ourmazd, *Phys. Rev. B*, *39* (1989) 3741.
12 S. Froyen, D. M. Wood and A. Zunger, *Appl. Phys. Lett.*, *54* (1989) 2435.
13 R. Zachai, E. Friess, G. Abstreiter, E. Kasper and H. Kibbel, *Proc. Int. Conf. on Physics of Semiconductors, '88, Warsaw*, in the press.
14 J. Ihm, A. Zunger and M. L. Cohen, *J. Phys. C: Solid State Phys.*, *12* (1979) 4409.
15 O. H. Nielsen and R. M. Martin, *Phys. Rev. B*, *32* (1985) 3780.
16 G. Kerker, *J. Phys. C: Solid State Phys.*, *13* (1980) L189.
17 D. J. Chadi and M. L. Cohen, *Phys. Rev. B*, *8* (1973) 5747.
18 S. Froyen, *Phys. Rev. B*, *39* (1989) 3168.
19 P. Hohenberg and W. Kohn, *Phys. Rev. B*, *864* (1964) 136.
20 W. Kohn and L. J. Sham, *Phys. Rev. A*, *140* (1965) 1133.
21 J. P. Perdew and A. Zunger, *Phys. Rev. B*, *23* (1981) 5048.
22 R. W. G. Wyckoff, *Crystal Structures, Vol. 1*, Wiley, New York, 2nd edn., 1963.

23 S.-H. Wei and A. Zunger, *Appl. Phys. Lett.*, *53* (1988) 2077.
24 C. G. Van de Walle and R. M. Martin, *Phys. Rev. B*, *34* (1986) 5621.
25 F. H. Pollak and M. Cardona, *Phys. Rev.*, *172* (1968) 816.
26 M. Tinkham, *Group Theory and Quantum Mechanics*, McGraw-Hill, New York, 1964.